

**In situ Electrosynthesis of Anthraquinone Electrolytes in Aqueous Flow Batteries**

Journal:	<i>Green Chemistry</i>
Manuscript ID	GC-ART-07-2020-002236.R1
Article Type:	Paper
Date Submitted by the Author:	17-Aug-2020
Complete List of Authors:	Jing, Yan; Harvard University Department of Chemistry and Chemical Biology, Chemistry Wu, Min; Harvard School of Engineering and Applied Sciences Wong, Andrew; Harvard School of Engineering and Applied Sciences, Applied Physics Fell, Eric; Harvard University, School of Engineering and Applied Sciences Jin, Shijian; Harvard School of Engineering and Applied Sciences, Material Science Pollack, Daniel; Harvard University, Department of Physics Kerr, Emily; Harvard University, Department of Chemistry and Chemical Biology Gordon, Roy; Harvard University, Department of Chemistry and Chemical Biology Aziz, Michael; Harvard School of Engineering and Applied Sciences,

1 ***In situ* Electrosynthesis of Anthraquinone Electrolytes in Aqueous Flow Batteries**

2 Yan Jing,^{1§} Min Wu,^{2§} Andrew A. Wong,² Eric M. Fell,² Shijian Jin,² Daniel A. Pollack,³ Emily
3 F. Kerr,¹ Roy G. Gordon,^{*,1,2} Michael J. Aziz^{*,2}

4 ¹ Department of Chemistry and Chemical Biology, Harvard University, Cambridge,
5 Massachusetts 02138, United States

6 ² John A. Paulson School of Engineering and Applied Sciences, Harvard University, Cambridge,
7 Massachusetts 02138, United States

8 ³ Department of Physics, Harvard University, Cambridge, Massachusetts 02138, United States

9 § These authors contributed equally to this work.

10 * Correspondence: gordon@chemistry.harvard.edu; maziz@harvard.edu

11 **Abstract**

12 We demonstrate the electrochemical oxidation of an anthracene derivative to a redox-active
13 anthraquinone at room temperature in a flow cell without the use of hazardous oxidants or noble
14 metal catalysts. The anthraquinone, generated *in situ*, was used as the active species in a flow
15 battery electrolyte without further modification or purification. This potentially scalable, safe,
16 green, and economical electrosynthetic method is also applied to another anthracene-based
17 derivative and may be extended to other redox-active aromatics.

18 **Introduction**

19 Aqueous redox flow batteries (ARFBs) represent a class of devices for storing electrical energy
20 that are especially well suited for large-scale stationary deployment.^{1, 2} Vanadium redox flow
21 batteries, the most developed ARFB technology, have been limited by the high and fluctuating
22 price of vanadium.³

23 Anthraquinone-based aqueous redox flow batteries are considered as one class of the most
24 promising alternatives to vanadium redox flow batteries because they can be composed of earth-
25 abundant elements such as C, H, O, and N while providing comparable electrochemical
26 performance.⁴⁻⁹ However, reducing the production cost of anthraquinone-based electrolytes and

27 improving their chemical stability are two major challenges preventing them from being cost-
28 competitive.⁹⁻¹⁴ Many factors can influence the synthesis cost of an organic molecule, including
29 the number, duration, complexity, and yields of the reaction steps, the reaction conditions (time,
30 temperature, and pressure), solvent and precursor costs, the cost of waste disposal, and economies
31 of scale. Likewise, a host of factors contributes to the stability, and by extension the long-term
32 viability, of redox-active organics including the chemical structure, solvent conditions, applied
33 potentials, and state of charge. Only through careful consideration of all of these factors can
34 commercial-scale organic ARFBs be viable storage solutions. Therefore, not only is the
35 development of a stable anthraquinone important, but the design of a potentially economical,
36 scalable, and green synthetic route toward targeted molecules is equally significant.^{11, 15}

37 Electrochemically-mediated synthesis (electrosynthesis) enables the replacement of hazardous
38 oxidizing and reducing agents by electric current, or “clean” electrons, through an electrode and
39 has attracted considerable attention for both laboratory and industrial applications in multiple
40 fields of research.¹⁶⁻²¹ Compared to traditional thermochemical synthesis, electrosynthesis can be
41 significantly more environmentally benign due to reduced waste production and alternative
42 chemicals consumed.^{22, 23} However, the necessity of using specific solvents combined with
43 supporting electrolytes, along with their subsequent separations, are some of the primary hurdles
44 limiting the feasibility of electrosynthesis compared to thermochemical processes in many cases.¹⁶

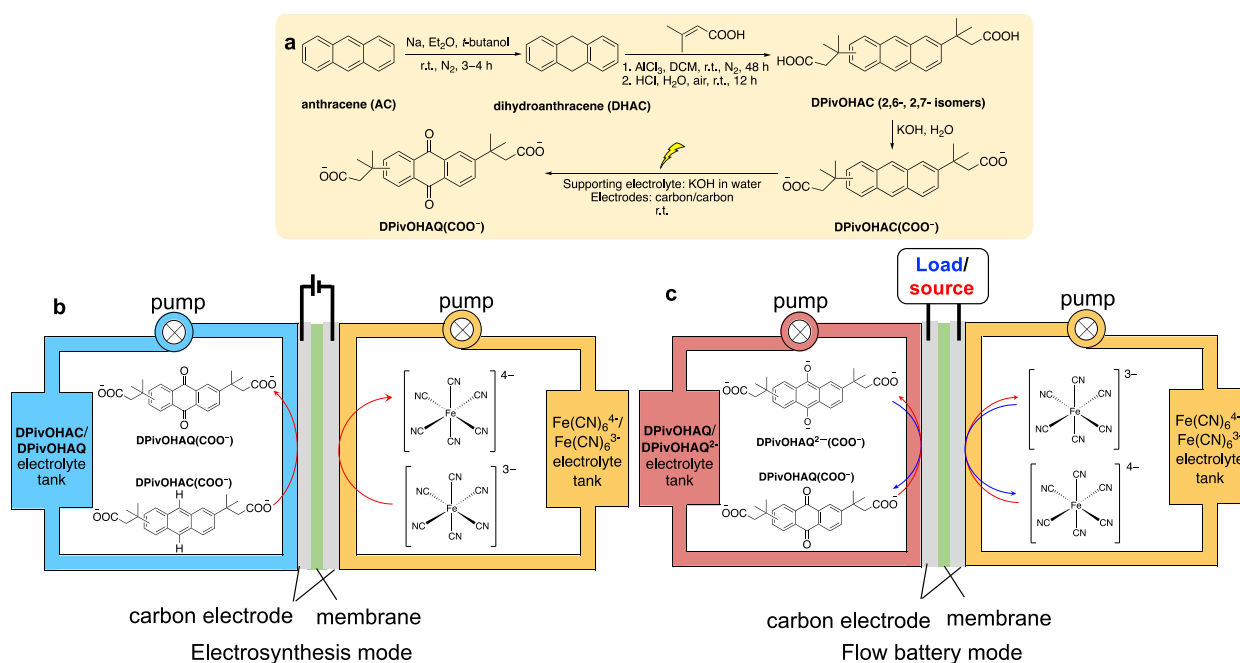
45 As an example, anthraquinone is typically produced from anthracene, an inexpensive and
46 abundant component of coal tar and petroleum.²⁴ Typically, hazardous oxidants such as
47 cerium(IV), chromium(VI), and vanadium(V) compounds dissolved in strong acids, sometimes at
48 elevated temperatures, are used to facilitate this thermochemical conversion.²⁵ To minimize the
49 use of hazardous materials, often these consumed oxidants are electrochemically regenerated and

50 reused for chemical oxidations,²⁵⁻³⁰ that is, a mediated or indirect electrochemical oxidation.
51 However, in both thermochemical conversion and mediated (indirect) electrochemical conversion,
52 isolating anthraquinone from these hazardous solutions can be time- and capital-intensive. Electro-
53 oxidations of anthracene and its derivatives at ~1 mM concentration have been performed
54 previously; however, the low concentrations of anthracene substrates and poor selectivity of the
55 reactions have prevented the method from being synthetically useful.³¹⁻³⁶

56 Using a scalable flow cell setup,³⁷ we demonstrate the capability to electrochemically oxidize
57 water-soluble anthracenes directly to anthraquinones in electrolytes without the use of strong
58 oxidants or catalysts, producing the desired negolyte (negative electrolyte) and ferrocyanide
59 posolyte (positive electrolyte) *in situ*. Compared to conventional thermochemical and
60 electrochemical methods, the new method is safe and potentially inexpensive because it eliminates
61 both the use of hazardous oxidants and the necessity of post-synthesis isolation of the products
62 from the supporting electrolytes. Taking advantage of a flow cell and bulk electrolysis setup, the
63 demonstrated electrosynthetic method is amenable to both continuous and batch processing.
64 Furthermore, we confirmed that the electrosynthetic method can also be extended to other
65 anthracene derivatives.

66 3,3'-(9,10-anthraquinone-diyl)bis(3-methylbutanoic acid) (**DPivOHAQ**) was recently reported
67 as an extremely stable and potentially inexpensive negolyte active species for organic ARFBs.³⁸
68 However, the use of CrO₃ in the synthesis can be highly toxic and explosive if produced in large
69 scale. Figure 1a shows the synthetic route for **DPivOHAQ** in three steps: 1) Through Birch
70 reduction, anthracene (**AC**) is converted to 9,10-dihydroanthracene (**DHAC**) at room temperature
71 (Figure S1). 2) After a Friedel–Crafts reaction and subsequent oxidation by air in one pot, two
72 water-soluble groups are introduced and **DHAC** is re-oxidized to an **AC** derivative (Figure S2),

73 forming 3,3'-(anthracene-diyl)bis(3-methylbutanoic acid) (**DPivOHAC**). The **DPivOHAC**
 74 powder was then dissolved in water by adding KOH to deprotonate the carboxylic acid groups. 3)
 75 Lastly, **DPivOHAQ** negolyte active species is produced by electrochemical oxidation in an
 76 aqueous electrolyte without the need for further purification. Figure 1b illustrates how
 77 **DPivOHAQ** and ferrocyanide active species can be produced *in situ* in the flow cell's
 78 electrosynthesis mode. These materials can directly serve as the active species in the negolyte and
 79 the posolyte, respectively, of a flow battery in the same cell as illustrated in Figure 1c.

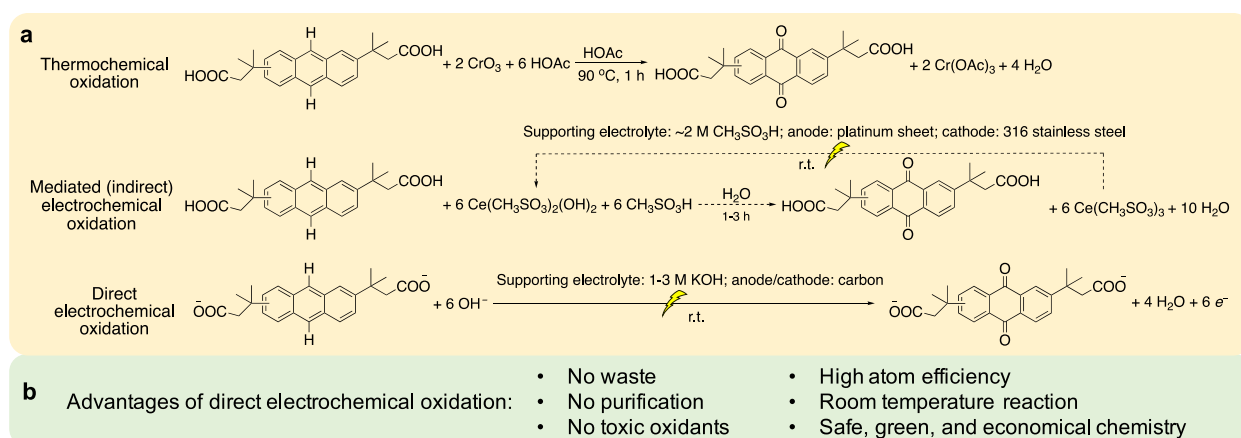


80

81 **Figure 1. Preparation of DPivOHAQ and the corresponding flow battery.** (a) The
 82 **DPivOHAQ** synthetic route and conditions starting from anthracene. (b) The setup for
 83 electrosynthesis of **DPivOHAQ** and ferrocyanide. (c) The flow battery setup with **DPivOHAQ**
 84 negolyte (generated *in situ*) and ferrocyanide posolyte (generated *in situ*). **DPivOHAC**: 3,3'-
 85 (anthracene-diyl)bis(3-methylbutanoic acid); **DPivOHAC(COO⁻)** is deprotonated **DPivOHAC**.
 86 **DPivOHAQ**: 3,3'-(9,10-anthraquinone-diyl)bis(3-methylbutanoic acid); **DPivOHAQ(COO⁻)** is
 87 deprotonated **DPivOHAQ**.

88 Figure 2a lists three different oxidation methods for **DPivOHAQ** synthesis. Conventionally,
 89 anthracene derivatives can be chemically oxidized to their anthraquinone forms by oxidants such
 90 as chromium oxide (CrO₃) in strong acidic media at elevated temperature.³⁸ To minimize the use

91 of hazardous oxidants, the strategy of mediated electrochemical oxidation can be performed by
 92 regenerating oxidants such as cerium(IV) compounds.^{26, 29} However, in both of these
 93 thermochemical and indirect electrochemical oxidation processes, tedious and expensive isolation
 94 of anthraquinone-based products from oxidants and acids is required. Taking advantage of the high
 95 solubility of **DPivOHAC** in base, we demonstrate a synthetic route via direct electrochemical
 96 oxidation in alkaline electrolyte with a flow cell. This method allows the complete elimination of
 97 hazardous oxidants and costly separation processes.



98

99 **Figure 2. Comparison of DPivOHAQ synthetic methods.** (a) Thermochemical, mediated
 100 (indirect) electrochemical, and direct electrochemical oxidation reactions to synthesize
 101 **DPivOHAQ**. (b) Advantages of direct electrochemical oxidation *in situ*.

102

103 Experimental

104 Cell hardware

105 Glassy carbon was used as the working electrode for all three-electrode cyclic voltammetry (CV)
 106 tests with a 5 mm diameter glassy carbon working electrode, an Ag/AgCl reference electrode
 107 (BASi, pre-soaked in 3 M NaCl solution), and a graphite counter electrode. Both undivided cell
 108 and divided cell were built for electrosynthesis. Flow battery experiments were constructed with
 109 cell hardware from Fuel Cell Tech (Albuquerque, NM) assembled into a zero-gap flow cell
 110 configuration. Pyrosealed POCO graphite flow plates with serpentine flow patterns were used for

111 both electrodes. Each electrode comprised a 5 cm² geometric surface area covered by AvCarb
112 HCBA woven carbon fiber without pretreatment, or Pt-coated Toray carbon paper without
113 pretreatment. The membrane is pre-soaked (1 M KOH for 24 hours) Nafion 212.

114 *Undivided electrolytic cell setup (electrochemical oxidation vs. the HER)*

115 Working electrode: carbon felt, where **DPivOHAC(COO⁻)** was oxidized to **DPivOHAQ(COO⁻)**;
116 counter electrode: carbon rod, where water was reduced to hydrogen gas. While the electrolyte
117 was stirred, a constant potential (1.1 V vs. Ag/AgCl) was applied to the divided electrolytic cell
118 until 120% of the required coulombs were extracted from the working electrode.

119 *Divided electrolytic cell setup (electrochemical oxidation vs. the ORR)*

120 Anode: Commercial AvCarb HCBA (woven carbon cloth), where **DPivOHAC(COO⁻)** was
121 oxidized to **DPivOHAQ(COO⁻)**; cathode: platinum coated Toray carbon paper, where humidified
122 air/oxygen was reduced to hydroxide. A constant voltage (1.8 V) was applied to the divided
123 electrolytic cell until the current decreased to 2 mA/cm². The number of extracted electrons was
124 ~1.2 times higher than the theoretical value.

125 *Divided electrolytic cell setup (electrochemical oxidation vs. the reduction of ferricyanide)*

126 Anode: AvCarb HCBA (woven carbon cloth), where **DPivOHAC(COO⁻)** was oxidized to
127 **DPivOHAQ(COO⁻)**; cathode: AvCarb HCBA (woven carbon cloth), where potassium
128 ferricyanide was reduced to potassium ferrocyanide. A constant current density (20 mA/cm²) was
129 applied to the divided cell for at most 1.5 hours with a 1.2 V voltage cutoff; when either time or
130 voltage reached the limit, the potential was held (1.2 V vs. ferro-/ferricyanide) until the current
131 decreased to 2 mA/cm². The number of extracted electrons was ~1.2 times higher than the
132 theoretical value.

133 An aliquot (~250 μL) was transferred from the as-prepared anolyte to an Eppendorf® tube
134 (capacity: 1.5 mL) and acidified by a drop of concentrated HCl to obtain **DPivOHAQ** precipitate.
135 The final **DPivOHAQ** precipitate was re-dissolved in $\text{DMSO-}d_6$ for ^1H NMR measurement. The
136 yield was determined by peak integrations of spectrum. Faradaic efficiency (%) = yield (%) / 1.2.
137 More detailed information can be found in the Supplementary information.

138 **Results and Discussion**

139 In an electrolytic cell, an anodic oxidation half reaction must be accompanied by a cathodic
140 reduction half reaction. As shown in Table 1, we devise three different reduction half reactions to
141 be coupled with direct **DPivOHAC** electrochemical oxidation, *i.e.*, the hydrogen evolution
142 reaction (HER), the oxygen reduction reaction (ORR), and the $\text{Fe}(\text{CN})_6^{3-}$ to $\text{Fe}(\text{CN})_6^{4-}$ reduction
143 reaction. The corresponding oxidation or reduction potentials for these reactions are listed in Table
144 1.

145 For the electrochemical oxidation of **DPivOHAC** to **DPivOHAQ**, two cell types are used, as
146 diagramed and described in Figures S3 and S4. A divided cell uses an ion exchange membrane to
147 separate the two half reactions, resembling the architecture of traditional fuel cells and ARFBs.
148 An undivided cell employs two electrodes suspended in electrolyte without the use of a membrane,
149 reflecting a bulk electrolysis cell.

150 Comparing these three overall reactions, the first one paired with the HER requires the highest
151 voltage; the second one paired with the ORR is known to have slow reaction kinetics and a high
152 overpotential;³⁹ the third one paired with $\text{Fe}(\text{CN})_6^{3-}$ to $\text{Fe}(\text{CN})_6^{4-}$ reduction exhibits the lowest
153 overall reaction cell voltage, suggesting the least amount of energy will be required for
154 electrosynthesis. Another merit of the third reaction is the *in situ* generation of the desired negolyte
155 active species (**DPivOHAQ**) and posolyte active species $\text{Fe}(\text{CN})_6^{4-}$ simultaneously. The

156 disadvantage is that at least six equivalents of ferricyanide and hydroxide are used. Given the
 157 similar reduction potentials of the ORR and of ferricyanide to ferrocyanide, an important direction
 158 for future research is the concurrent reduction of oxygen and ferricyanide in order to achieve high
 159 yields as well as lower ferricyanide usage. By using the same full cell configuration without
 160 changing electrolyte reservoirs, carbon-based electrodes, or ion-exchange membranes, we can
 161 immediately switch from electrosynthesis mode to flow battery mode for electrochemical energy
 162 storage. In this configuration, neither hazardous oxidants nor purification steps are needed, nor is
 163 waste generated. Furthermore, the reaction may proceed at room temperature with high atom
 164 efficiency. The new synthesis is therefore potentially safe, green, economical, and scalable.

165 **Table 1.** Anodic, cathodic, and overall reactions for direct electrochemical oxidation.

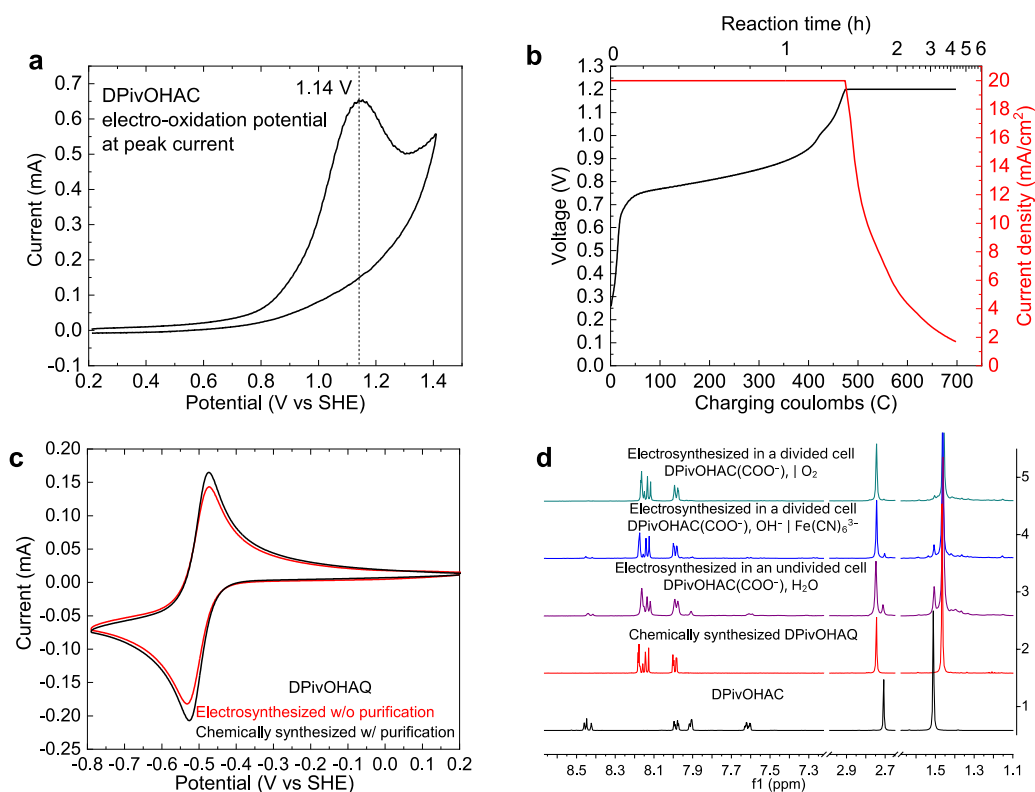
	Reactions	Potential at pH 14 (V vs SHE) / Cell voltage (V)
Anodic	$\text{DPivOHAC}(\text{COO}^-) + 6 \text{OH}^- \longrightarrow \text{DPivOHAQ}(\text{COO}^-) + 4 \text{H}_2\text{O} + 6 e^-$	1.14*
Cathodic	$6 \text{H}_2\text{O} + 6 e^- \longrightarrow 3 \text{H}_2 + 6 \text{OH}^-$ (divided or undivided cell)	-0.83
	$1.5 \text{O}_2 + 6 e^- + 3 \text{H}_2\text{O} \longrightarrow 6 \text{OH}^-$ (divided or undivided cell)	0.40
	$6 \text{Fe}(\text{CN})_6^{3-} + 6 e^- \longrightarrow 6 \text{Fe}(\text{CN})_6^{4-}$ (divided cell)	0.44
Overall	$\text{DPivOHAC}(\text{COO}^-) + 2 \text{H}_2\text{O} \longrightarrow \text{DPivOHAQ}(\text{COO}^-) + 3 \text{H}_2$	1.97
	$\text{DPivOHAC}(\text{COO}^-) + 1.5 \text{O}_2 \longrightarrow \text{DPivOHAQ}(\text{COO}^-) + \text{H}_2\text{O}$	0.74
	$\text{DPivOHAC}(\text{COO}^-) + 6 \text{OH}^- + 6 \text{Fe}(\text{CN})_6^{3-} \longrightarrow \text{DPivOHAQ}(\text{COO}^-) + 6 \text{Fe}(\text{CN})_6^{4-} + 4 \text{H}_2\text{O}$	0.70

166 *: The electro-oxidation potential at peak current

167 The cyclic voltammogram (CV) of **DPivOHAC** at pH 14 (Figure 3a) indicates a peak oxidation
 168 current at 1.14 V vs. SHE. This value is more positive than the standard redox potential of 0.40 V
 169 vs. SHE for the oxygen evolution reaction (OER), and we expect that the OER will be a major side
 170 reaction of electrosynthesis.

171 We then assembled a flow cell with **DPivOHAC** as the anolyte and $\text{K}_3\text{Fe}(\text{CN})_6$ as the catholyte.
 172 Galvanostatic electrolysis with a potentiostatic hold after reaching a potential limit of 1.2 V was
 173 performed for ~4.5 hours to complete the electrosynthesis. The OER side reaction, evidenced by

174 the observation of bubbles generated in the anolyte, precludes a faradaic efficiency of 100%. Thus,
 175 the number of electrons extracted from the anolyte was ~ 1.2 times higher than the theoretical
 176 number for complete conversion. A plateau appears at ~ 0.8 V against $\text{K}_3\text{Fe}(\text{CN})_6$ (0.44 V vs. SHE)
 177 in the voltage profile (Figure 3b).



178

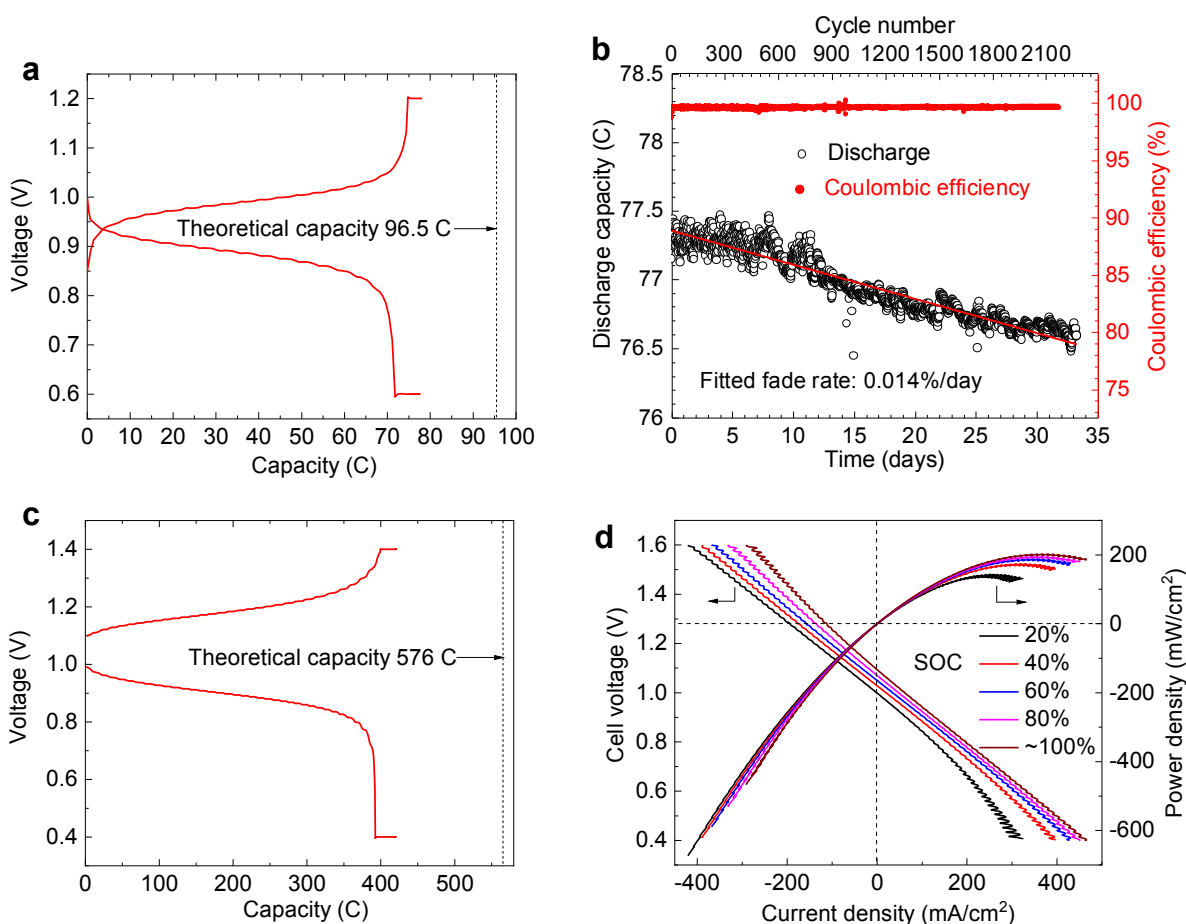
179 **Figure 3. Electrochemical synthesis and characterization of DPivOHAQ.** (a) The cyclic voltammogram
 180 (CV) of 0.1 M **DPivOHAC** in 1.0 M $\text{KCl} + 1.0$ M KOH aqueous solution. Scan rate: 0.1 V/s. (b)
 181 The electrochemical oxidation was conducted by using a constant current (20 mA/cm^2) with a
 182 subsequent potential hold (1.2 V) until the current density decreased to 2 mA/cm^2 . (c) CV of
 183 10 mM electro-synthesized **DPivOHAQ** (against $\text{Fe}(\text{CN})_6^{3-}$) without purification and 10 mM
 184 chemically synthesized **DPivOHAQ** with purification in 1 M KOH aqueous solutions,
 185 respectively. Scan rate: 0.1 V/s. (d) ^1H NMR spectra of (bottom to top): chemically synthesized
 186 **DPivOHAC** (black); chemically synthesized **DPivOHAQ** (red); electro-synthesized **DPivOHAQ**
 187 in an undivided cell (purple), 17.3% of **DPivOHAC** remained unreacted according to the
 188 integration, yield: 82.7% ; electro-synthesized **DPivOHAQ** in a divided cell against $\text{Fe}(\text{CN})_6^{3-}$
 189 (blue), 7.0% of **DPivOHAC** remained unreacted according to the integration, yield: 93.0% ;
 190 electro-synthesized **DPivOHAQ** in a divided cell against O_2 (green), 0% of **DPivOHAC** remained
 191 unreacted according to the integration, yield: 100% . The deuterated solvent is $\text{DMSO}-d_6$, and the
 192 solvent peaks (DMSO and H_2O) were removed to better display the peaks of interest. The

193 electrosynthetic details are described under the headings **Electrosynthesis I, II, and III** in the
194 Supporting Information.
195

196 We compared the CV of **DPivOHAQ** produced by electrosynthesis against the reduction of
197 $\text{Fe}(\text{CN})_6^{3-}$ to that of the chemically synthesized product at the same concentration to verify that
198 the reaction products are the same regardless of the synthetic procedure employed (Figure 3c). The
199 two CV curves show identical redox peaks and similar peak currents, indicating a high-yield
200 electrosynthesis process. ^1H nuclear magnetic resonance (NMR) spectroscopy was used to further
201 examine the structure of electrosynthesized **DPivOHAQ** when using either a divided or undivided
202 cell (Figure S3) and to compare the spectra with those of the starting material, **DPivOHAC**, and
203 the chemically synthesized **DPivOHAQ**. The top three spectra in Figure 3d are the ^1H NMR
204 spectra from electrosynthesized **DPivOHAQ**, in which the dominating peaks have the same
205 chemical shifts as those in the spectrum of chemically synthesized **DPivOHAQ**, further suggesting
206 the desired product was achieved.

207 Slightly different yields of **DPivOHAQ** were obtained when paired with the HER in an
208 undivided cell or with $\text{Fe}(\text{CN})_6^{3-}$ reduction or the ORR in a divided cell (Figure S4). The 82.7%
209 yield when paired with the HER in an undivided cell could be explained by a molecular shuttling
210 effect; *i.e.*, the electrosynthesized **DPivOHAQ** can first migrate to the cathode where it is reduced,
211 then diffuse back to the anode for re-oxidation. As a result, double counting of electrons can occur.
212 When paired with the $\text{Fe}(\text{CN})_6^{3-}$ reduction half reaction, a yield of 93.0% was obtained. The
213 incomplete yield is likely due to the consumption and therefore decreased concentration of both
214 **DPivOHAC** and OH^- as the electrosynthesis continues, making further oxidation increasingly
215 difficult.

216 The use of the ORR half reaction achieved almost 100.0% yield. This exceptional yield may be
 217 attributed to the as-formed OH^- ions on the cathode (ORR) side crossing over to the anolyte and
 218 compensating for any loss of OH^- ions on the anode side. Overall yields in excess of 80.0% for all
 219 three conditions exceed many conventional reactions and are acceptable for direct flow battery use
 220 without purification or separation.



221

222 **Figure 4. Full cell performance evaluation from Electrosynthesis III and IV.** (a) A
 223 representative charge–discharge profile with 0.1 M DPivOHAQ. Negolyte: 5 mL of 0.1 M
 224 DPivOHAQ pH = ~13.5. Posolyte: 100 mL of 0.1 M potassium ferro-/ferricyanide solution [~0.06
 225 M $\text{K}_4\text{Fe}(\text{CN})_6$ and ~0.04 M $\text{K}_3\text{Fe}(\text{CN})_6$] pH = ~13.6. (b) Discharge capacity (C) and coulombic
 226 efficiency (%) vs. cycle number and time (days). Negolyte: 4.5 mL of 0.1 M DPivOHAQ. Posolyte:
 227 100 mL of 0.1 M ferro-/ferricyanide solution [~0.06 M $\text{K}_4\text{Fe}(\text{CN})_6$ and ~0.04 M $\text{K}_3\text{Fe}(\text{CN})_6$].
 228 Current density: 30 mA/cm² with potential hold (cutoffs: 0.6 V, 1.2 V) until current decreased to
 229 2 mA/cm². (c) A representative charge–discharge profile with 0.5 M DPivOHAQ. Negolyte: 6
 230 mL of 0.5 M DPivOHAQ. Posolyte: 100 mL of 0.5 M potassium ferro-/ferricyanide solution [~0.3

231 M $\text{K}_4\text{Fe}(\text{CN})_6$ and ~ 0.2 M $\text{K}_3\text{Fe}(\text{CN})_6$]. Current density: 100 mA/cm^2 with potential hold (cutoff:
232 0.4 V, 1.4 V) until current decreased to 2 mA/cm^2 . (d) Polarization curves of the 0.5 M
233 **DPivOHAQ** at the SOC of 20%, 40%, 60%, 80%, and $\sim 100\%$ respectively. Descriptions of
234 **Electrosynthesis III** and **IV** can be found in the Supporting Information.

235
236 To demonstrate the feasibility of switching from the electrosynthesis mode (when paired with
237 $\text{Fe}(\text{CN})_6^{3-}$ reduction) to flow battery mode, we began charge–discharge cycling immediately upon
238 completion of the electrosynthesis, without performing any purification. Because other research
239 has reported that quinones and related compounds can decompose in the presence of light,^{40–42} we
240 wrapped the electrolyte reservoirs with aluminum foil to avoid light-induced decomposition during
241 cell cycling (Figures S13–S15). Figure 4a shows the charge–discharge profile of a single cycle
242 with an open circuit voltage of ~ 1.0 V and a capacity of 84.0 coulombs. Given the 93.0% yield
243 found from the ^1H NMR, the capacity utilization is 93.6%. Long-term cycling was then performed
244 to determine a temporal capacity fade rate of the full cell. Figure 4b demonstrates the discharge
245 capacity and coulombic efficiency over 33.2 days and 2271 cycles with a fitted fade rate of
246 0.014%/day and an average coulombic efficiency of 99.53%. This is consistent with the fade rate
247 of chemically synthesized **DPivOHAQ**.³⁸ The extremely low capacity fade rate is attributed to the
248 chemical stability of the molecular structure. The C–C covalent bond between the anthraquinone
249 core and the functionalizing chains is more robust in strong base and at elevated temperature than
250 the C–O bond demonstrated in previous work.^{4, 5, 38} Furthermore, the two branched methyl groups
251 on the carbon connected to the anthraquinone (AQ) core may increase the stability of the
252 solubilizing chain even when exposed to harsh conditions.¹⁵

253 To examine the feasibility of this method for potential industry use, we further conducted
254 electrosynthesis with a higher concentration (0.5 M) of **DPivOHAC** at a higher current density
255 (100 mA/cm^2) (See Figure S5). Figure 4c shows that 0.5 M electrosynthesized negolyte can deliver
256 72.9% of the theoretical capacity. We attribute the discrepancy between the delivered capacity and

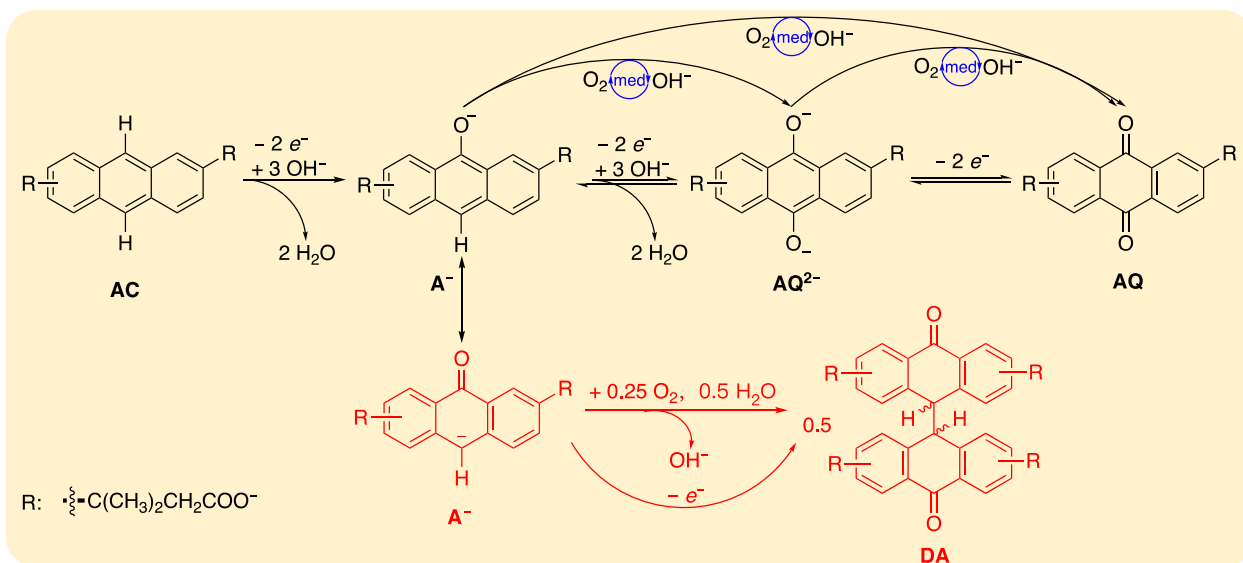
257 the theoretical capacity primarily to incomplete conversion (Figure S6). The capacity utilization is
258 81.9% if we consider that there is 11.0% unreacted **DPivOHAC(COO⁻)** in the negolyte.
259 Additionally, the mass transport of active species at 0.5 M concentration may be another issue
260 limiting the full capacity utilization. The corresponding polarization curve at different states of
261 charge (SOC) is shown in Figure 4d. The peak power density exceeds 0.2 W/cm² when at ~100 %
262 of SOC.

263 Given the total transfer of six electrons during the electrosynthesis of **DPivOHAC** to
264 **DPivOHAQ**, the high yields achieved in this work might be surprising. We hypothesize a three-
265 step successive two-electron transfer mechanism^{34,35}: first, when a potential is applied, anthracene
266 (**AC**) may react with three OH⁻ ions and donate two electrons to produce two water molecules and
267 the anthrone anion (**A⁻**); second, **A⁻** may further react with another three OH⁻ ions and donate
268 another two electrons to generate two water molecules and the deprotonated anthrahydroquinone
269 dianion (**AQ²⁻**); third, **AQ²⁻** may further release two electrons to afford the anthraquinone species
270 (**AQ**). Complete electrochemical conversion in the third step has been well-documented at
271 negative potentials vs. ferro-/ferricyanide^{1,2,43} and should therefore be rapid at positive potentials
272 vs. ferro-/ferricyanide. The reverse reaction of the second step has recently been identified as a
273 side reaction in ARFBs, and the forward reaction is chemically feasible when exposed to O₂ or
274 air.^{14,38} Given the high voltage applied to the cell, it is thus plausible that the forward reactions
275 (**AC** to **A⁻** to **AQ²⁻**/**AQ**) can electrochemically proceed completely and swiftly.

276 Our group has also previously proposed a side reaction pathway for anthraquinones,^{14,44} where
277 the anthrone anion (**A⁻**) can be oxidatively dimerized to dianthrone (**DA**) chemically and/or
278 electrochemically. According to ¹H NMR spectra (Figure 3d) and liquid chromatography–mass
279 spectrometry (LC–MS) results (Figure S7), neither **DA** nor Kolbe electrolysis-related byproducts⁴⁵

280 were detected (Scheme S1), suggesting that **AC/AQ**-related side reactions can be negligible when
281 a sufficient OH^- concentration is present to prevent dianthrone formation and a sufficiently low
282 voltage cutoff is chosen to prevent Kolbe electrolysis dimer formation. The major competing side
283 reaction is the OER, which, along with the reactions of **AC** to **A⁻** to **AQ²⁻**, will consume OH^- and
284 may lead to the formation of **DA** as a result of insufficient OH^- ions in the **DPivOHAC** solution
285 (see **Electrosynthesis V** in the SI). Interestingly, the dianthrone (Scheme S2), detected by
286 LC–MS (Figure S11), are surprisingly redox-active when a broad voltage window is applied
287 (Figures S8 and S9 and Scheme S2). On the one hand, the OER can reduce faradaic efficiency; on
288 the other hand, the generated oxygen can serve as a mediator and chemically oxidize intermediates
289 (*i.e.*, **A⁻**, **AQ²⁻**) to the final **AQ** form, *i.e.*, mediated (indirect) electrochemical oxidation. Because
290 the entire process involves not only electrochemical oxidations, but also chemical oxidations, it is
291 more appropriate to call it an electrochemical–chemical oxidation process.⁴⁶

292 In the proposed mechanism, the anthrone derivative is an intermediate in the electrochemical
293 oxidation. Anthrone formation has been identified as the major side reaction causing capacity fade
294 in previous work;^{14, 38} therefore, it is plausible that lost capacity of anthraquinone flow battery
295 systems may be recovered and anthraquinone lifetime extended by electrochemically oxidizing
296 anthrone to redox-active anthraquinone derivatives.



297

298 **Scheme 1. Proposed electrochemical oxidation mechanism.** Three-step successive two-electron
 299 transfer process from AC to A⁻, A⁻ to AQ²⁻, and AQ²⁻ to AQ. The generated oxygen from the
 300 OER side reaction may incur chemical oxidation processes including A⁻ to AQ²⁻, AQ²⁻ to AQ,
 301 and oxidative dimerization (A⁻ to DA).

302

303 To demonstrate that the electrochemical oxidation can be applied to other anthracene
 304 derivatives, we performed electrochemical oxidation of 4,4'-(9,10-dihydroanthracene-
 305 diyl)dibutanoic acid (**DBDHAC**), where the molecular core is 9,10-dihydroanthracene.³⁸ The ¹H
 306 NMR results indicate that **DBDHAC** can, like **DPivOHAC**, be electrochemically oxidized to the
 307 final anthraquinone (Figure S12), **DBAQ** (4,4'-(9,10-anthraquinone-diyl)dibutanoic acid), which
 308 has also been shown to be extremely stable.³⁸

309 The shared precursor of **DPivOHAQ** and **DBAQ**, anthracene, is abundant in crude petroleum
 310 and coal tar, and can be synthesized from benzene and benzyl alcohol (Scheme S3).⁴⁷ The
 311 precursor of **DPivOHAQ**, 3,3'-dimethyl acrylic acid, can be industrially produced from malonic
 312 acid, a food acid; the precursor of **DBAQ**, succinic anhydride, can be industrially hydrogenated
 313 from maleic anhydride and used as an important intermediate on an industrial scale. Thus, both
 314 **DPivOHAQ** and **DBAQ** can be readily synthesized from commodity chemicals. Although the
 315 synthetic cost of **DPivOHAQ** or **DBAQ** should be somewhat higher than that of 2,6-

316 dihydroxyanthraquinone (**DHAQ**) due to more steps and more chemicals involved, the capital cost
317 of AORFBs that utilize finite-lifetime electrolytes can be viewed as including the total active cost,
318 which is the sum of the initial cost of redox-active materials and the present value of the future
319 costs of periodic electrolyte replacement.¹³ This can lead to an initial cost—lifetime trade-off in
320 the choice of electrolytes. Over an extended operational lifetime, the total active cost of
321 **DPivOHAQ** or **DBAQ** may be less than that of **DHAQ** due to their much longer lifetimes.¹⁴

322 **Conclusion**

324 This work demonstrates a potentially scalable, safe, green, and economical *in situ*
325 electrosynthetic method for anthraquinone electrolytes in a flow cell without the use of hazardous
326 oxidants or precious metal catalysts. The as-generated electrolytes, which are extremely stable,
327 can be immediately used in a redox flow battery without separation or purification. Other low-cost
328 compounds may also be amenable to this approach, providing a pathway to lower the cost of
329 electrochemical grid storage systems, thereby accelerating the development of a renewable energy
330 economy. The technique extends the opportunities for direct aqueous electrosynthesis to replace
331 thermochemical synthesis of value-added organics.

332 **Supplementary Information**

333 Supplementary Information can be found with this article online at

334 **Acknowledgments**

335 This research was supported by U.S. DOE award DE-AC05-76RL01830 through PNNL
336 subcontract 428977, Innovation Fund Denmark via the Grand Solutions project "ORBATS" file
337 no. 7046-00018B, and NSF grant CBET-1914543. D.A.P. acknowledges funding support from the
338 NSF Graduate Research Fellowship Program, no. DGE1144152 and DGE1745303.

339 **Declaration of Interests**

340 Harvard University has filed a patent application on the materials and the electrosynthetic methods
341 described in this paper.

342

343

REFERENCES

- 344 1. B. Huskinson, M. P. Marshak, C. Suh, S. Er, M. R. Gerhardt, C. J. Galvin, X. Chen, A. Aspuru-
345 Guzik, R. G. Gordon and M. J. Aziz, *Nature*, 2014, **505**, 195–198.
- 346 2. K. Lin, Q. Chen, M. R. Gerhardt, L. Tong, S. B. Kim, L. Eisenach, A. W. Valle, D. Hardee, R. G.
347 Gordon, M. J. Aziz and M. P. Marshak, *Science*, 2015, **349**, 1529–1532.
- 348 3. M. Moore, R. Counce, J. Watson and T. Zawodzinski, *Journal of Advanced Chemical*
349 *Engineering*, 2015, **5**, doi:10.4172/2090-4568.1000140.
- 350 4. D. G. Kwabi, K. Lin, Y. Ji, E. F. Kerr, M.-A. Goulet, D. De Porcellinis, D. P. Tabor, D. A.
351 Pollack, A. Aspuru-Guzik, R. G. Gordon and M. J. Aziz, *Joule*, 2018, **2**, 1894–1906.
- 352 5. Y. Ji, M.-A. Goulet, D. A. Pollack, D. G. Kwabi, S. Jin, D. De Porcellinis, E. F. Kerr, R. G.
353 Gordon and M. J. Aziz, *Adv. Energy Mater.*, 2019, **9**, 1900039.
- 354 6. A. Hollas, X. Wei, V. Murugesan, Z. Nie, B. Li, D. Reed, J. Liu, V. Sprenkle and W. Wang,
355 *Nature Energy*, 2018, **3**, 508–514.
- 356 7. C. Wang, X. Li, B. Yu, Y. Wang, Z. Yang, H. Wang, H. Lin, J. Ma, G. Li and Z. Jin, *ACS Energy*
357 *Letters*, 2020, **5**, 411–417.
- 358 8. J. D. Hofmann, F. L. Pfanschilling, N. Krawczyk, P. Geigle, L. Hong, S. Schmalisch, H. A.
359 Wegner, D. Mollenhauer, J. Janek and D. Schröder, *Chemistry of Materials*, 2018, **30**, 762–774.
- 360 9. D. G. Kwabi, Y. Ji and M. J. Aziz, *Chem. Rev.*, 2020, **120**, doi.org/10.1021/acs.chemrev.9b00599.
- 361 10. Z. Yang, L. Tong, D. P. Tabor, E. S. Beh, M.-A. Goulet, D. De Porcellinis, A. Aspuru-Guzik, R.
362 G. Gordon and M. J. Aziz, *Adv. Energy Mater.*, 2018, **8**, 1702056.
- 363 11. V. Dieterich, J. D. Milshtein, J. L. Barton, T. J. Carney, R. M. Darling, F. R. Brushett,
364 *Translational Materials Research*, 2018, **5**, 034001.
- 365 12. S. Jin, E. M. Fell, L. Vina-Lopez, Y. Jing, P. W. Michalak, R. G. Gordon and M. J. Aziz, *Adv.*
366 *Energy Mater.*, 2020, **10**, doi.org/10.1002/aenm.202000100.
- 367 13. F. R. Brushett, M. J. Aziz and K. E. Rodby, *ACS Energy Letters*, 2020, **5**, 879–884.
- 368 14. M.-A. Goulet, L. Tong, D. A. Pollack, D. P. Tabor, S. A. Odom, A. Aspuru-Guzik, E. E. Kwan,
369 R. G. Gordon and M. J. Aziz, *J. Am. Chem. Soc.*, 2019, **141**, 8014–8019.
- 370 15. P. Anastas, N. Eghbali, *Chem. Soc. Rev.*, 2010, **39**, 301–312.
- 371 16. D. S. P. Cardoso, B. Šljukić, D. M. F. Santos, C. A. C. Sequeira, *Organic Process Research &*
372 *Development*, 2017, **21**, 1213–1226.
- 373 17. M. Yan, Y. Kawamata, P. S. Baran, *Chem. Rev.*, 2017, **117**, 13230–13319.
- 374 18. B. K. Peters, K. X. Rodriguez, S. H. Reisberg, S. B. Beil, D. P. Hickey, Y. Kawamata, M.
375 Collins, J. Starr, L. Chen, S. Udyavara, K. Klunder, T. J. Gorey, S. L. Anderson, M. Neurock, S.
376 D. Minteer and P. S. Baran, *Science*, 2019, **363**, 838–845.
- 377 19. E. J. Horn, B. R. Rosen, Y. Chen, J. Tang, K. Chen, M. D. Eastgate, P. S. Baran, *Nature*, 2016,
378 **533**, 77–81.
- 379 20. A. Badalyan, S. S. Stahl, *Nature*, 2016, **535**, 406–410.
- 380 21. G. G. Botte, *The Electrochemical Society Interface*, 2014, **23**, 49–55.
- 381 22. P. M. Bersier, L. Carlsson and J. Bersier, *Topics in Current Chemistry*, 1994, **170**, 116–136.
- 382 23. C. Xia, Y. Xia, P. Zhu, L. Fan and H. Wang, *Science*, 2019, **366**, 226–231.
- 383 24. M. Granda, C. Blanco, P. Alvarez, J. W. Patrick and R. Menendez, *Chem. Rev.*, 2014, **114**, 1608–
384 1636.
- 385 25. R. S. Tipson, in *National Bureau of Standards Monograph 87*, 1965, 1–49.
- 386 26. R. P. Kreh, R. M. Spotnitz and J. T. Lundquist, *J. Org. Chem.*, 1989, **54**, 1531–1535.
- 387 27. E. Oppermann, *US Pat.*, US823,435A, 1906.
- 388 28. E. Steckhan, in *Ullmann's Encyclopedia of Industrial Chemistry*, Wiley-VCH Verlag GmbH &
389 Co. KGaA, Weinheim, 2011, **12**, DOI: 10.1002/14356007.o09_o04.

- 390 29. R. M. Spotnitz, R. P. Kreh, J. T. Lundquist and P. J. Press, *Journal of Applied Electrochemistry*,
391 1990, **20**, 209–215.
- 392 30. R. P. Kreh, R. M. Spotnitz and J. T. Lundquist, *Tetrahedron Letters*, 1987, **28**, 1067–1068.
- 393 31. E. J. Majeski, J. D. Stuart and W. E. Ohnesorge, *J. Am. Chem. Soc.*, 1968, **90**, 633–636.
- 394 32. L. R. Faulkner, A. J. Bard, *J. Am. Chem. Soc.*, 1968, **90**, 6284–6290.
- 395 33. C. Amatore and A. R. Brown, *J. Am. Chem. Soc.*, 1996, **118**, 1482–1486.
- 396 34. O. Tovide, N. Jahed, C. E. Sunday, K. Pokpas, R. F. Ajayi, H. R. Makelane, K. M. Molapo, S. V.
397 John, P. G. Baker and E. I. Iwuoha, *Sensors and Actuators B: Chemical*, 2014, **205**, 184–192.
- 398 35. C. A. Paddon, C. E. Banks, I. G. Davies and R. G. Compton, *Ultrason. Sonochem.*, 2006, **13**,
399 126–132.
- 400 36. V. D. Parker, *Acta Chemica Scandinavica*, 1970, **24**, 2757–2767.
- 401 37. T. Noel, Y. Cao and G. Laudadio, *Acc. Chem. Res.*, 2019, **52**, 2858–2869.
- 402 38. M. Wu, Y. Jing, A. A. Wong, E. M. Fell, S. Jin, Z. Tang, R. G. Gordon and M. J. Aziz, *Chem*,
403 2020, **6**, 1432–1442.
- 404 39. R. W. Zurilla, R. K. Sen and E. Yeager, *J. Electrochem. Soc.*, 1978, **125**, 1103–1109.
- 405 40. G. Maier, L. H. Franz, H.-G. Hartan, K. Lanz and H. P. Reisenauer, *Chemische Berichte*, 1985,
406 **118**, 3196–3204.
- 407 41. S. A. Carlson and D. M. Hercules, *Analytical Chemistry*, 1973, **45**, 1794–1799.
- 408 42. B. E. Hulme, E. J. Land and G. O. Phillips, *J. Chem. Soc. Faraday Trans. 1*, 1972, **68**, 1992–
409 2002.
- 410 43. M. Quan, D. Sanchez, M. F. Wasylkiw and D. K. Smith, *J. Am. Chem. Soc.*, 2007, **129**, 12847–
411 12856.
- 412 44. S. Jin, Y. Jing, D. G. Kwabi, Y. Ji, L. Tong, D. De Porcellinis, M. A. Goulet, D. A. Pollack, R. G.
413 Gordon and M. J. Aziz, *ACS Energy Letters*, 2019, **4**, 1342–1348.
- 414 45. H.-J. Schäfer, *Topics in Current Chemistry*, 1990, **152**, 91–151.
- 415 46. C. Costentin and J.-M. Savéant, *Proc. Natl. Acad. Sci. U S A*, 2019, **116**, 11147–11152.
- 416 47. H. E. Ungnade and E. W. Crandall, *J. Am. Chem. Soc.*, 1949, **71**, 3009–3010.

417